

DOI: 10.1002/adma.200702567

Non-Volatile Organic Memory Applications Enabled by In Situ Synthesis of Gold Nanoparticles in a Self-Assembled Block Copolymer**

By Wei Lin Leong,* Pooi See Lee,* Anup Lohani, Yeng Ming Lam, Tupei Chen, Sam Zhang, Ananth Dodabalapur, and Subodh G. Mhaisalkar

Block copolymers have unique associative properties that facilitate self-assembly into nanostructures that have been widely used in soft lithography,^[1] templating,^[2] drug delivery,^[3] biomedical,^[4,5] and chemical catalytic^[6] applications. Of special interest is the in situ preparation of metallic or semiconducting nanoparticles in amphiphilic block copolymers.^[7–12] The synthesis of nanoparticles in block copolymer micelles solves the problem of particle size control and stabilization compared to classical stabilization systems that employ surfactants^[13–15] or microemulsions.^[16,17] Nanocrystal-based organic memories^[18–21] are attracting widespread interest owing to their simple structure and the prospect of creating 2D/3D stacks of these memory cells for increased bit densities. Recent reviews^[20,22,28] summarize the literature for these nanoparticle-based organic memories comprehensively, and have identified the main operating mechanisms to be one of the following: (i) an electric-field-induced charge transfer between the nanoparticles and the surrounding conjugated compounds,^[19,22] (ii) filamentary conduction,^[23,24] (iii) charge trapping–detrapping,^[25,26] and (iv) space-charge field inhibition of injection in the nanoparticles through a high-voltage pulse.^[20,27] Besides the widely used two-terminal bistable organic memory devices, an

alternative memory architecture that can be adopted is based on an organic thin-film transistor (OTFT) with a non-volatile floating gate memory^[29] which allows a direct integration of the memory element with the transistor for integrated circuit applications. The ability to have a one-step fabrication process to generate arrays of metallic nanoparticles using solution-processing methods makes this approach amenable to potential implementations in the nanoparticle-based organic memory devices mentioned above. This is in contrast to past designs of organic memory devices, which involved the use of multistep approaches of presynthesizing nanoparticles followed by surface modification to prevent agglomeration prior to embedding them in multiple functional layers through solution processing or physical vapor deposition. Furthermore, this solution-processing approach is especially suitable for low-cost, large-area processing on flexible substrates, which may be considered to be the cornerstone of organic electronics applications.

We demonstrate herein, for the first time, a polymeric memory that comprises an in situ synthesis strategy of gold nanoparticles in polystyrene-*block*-poly(4-vinylpyridine) (PS-*b*-P4VP). This system serves as a prototype for a generic memory device using nanoparticles as floating gate charge storage centers and, in particular, for integration into OTFT-based circuits. The block copolymer micelles turn out to be an excellent model system that is simple, forms a self-assembled ordered nanostructure, and provides optimum control over nanoparticle size formation and isolation. The response of the memory device is controlled by the applied voltage, where a spatial distribution of charge carriers can be retained (trapped) in the nanoparticles. Since any accumulation (or trapping) of charge will be reflected by a change in capacitance, one may study the memory behavior through capacitance–voltage (*C*–*V*) and transient capacitance measurements. The ability to tune the memory behavior was also illustrated by changing the loading of Au nanoparticles. The possibility to form a new organic transistor-based memory system was demonstrated using pentacene as the active organic semiconductor layer and the Au nanoparticles in self-assembled PS-*b*-P4VP as the charge storage components in a metal–pentacene–insulator–silicon (MPIS) configuration. These experiments extend the understanding and applicability of charge trapping using arrays of Au nanoparticles in block copolymer nanodomains. We believe that our work suitably

[*] W. L. Leong, Dr. P. S. Lee, Dr. A. Lohani, Dr. Y. M. Lam, Dr. S. G. Mhaisalkar
School of Materials Science and Engineering
Nanyang Technological University
50 Nanyang Drive, Singapore 639798 (Singapore)
E-mail: leon0043@ntu.edu.sg; pslee@ntu.edu.sg
Dr. T. P. Chen
School of Electrical and Electronic Engineering
Nanyang Technological University
50 Nanyang Drive, Singapore 639798 (Singapore)
Dr. S. Zhang
School of Mechanical and Aerospace Engineering
Nanyang Technological University
50 Nanyang Drive, Singapore 639798 (Singapore)
Dr. A. Dodabalapur
Microelectronic Research Center
University of Texas at Austin
Austin, TX 78712 (USA)

[**] This work is supported by A*Star and Nanyang Technological University (NTU) Singapore. The authors wish to acknowledge discussions with Dr. Beng Ong of the Institute of Materials Research and Engineering and NTU, and with Dr. Yuning Li of the Xerox Research Center of Canada. Supporting Information is available online from Wiley InterScience or from the authors.

illustrates the potential of a novel memory system, in which a wide range of block copolymers and metal or semiconducting nanoparticles can be combined to realize low-cost, solution-processable design and process schemes in memory applications. The choice of block copolymer can be tailor-made, as the volume fraction of each block and/or total molecular weight can be varied to create different types of tunneling barriers and hence utilized in different memory architectures and applications.

The block copolymer forms a micellar structure when dissolved in toluene owing to the preferential solubility of the non-polar PS block in toluene while the P4VP block, being insoluble, collapses to form the core of the micelle. The micellation process is illustrated in Figure 1a. The spin-coated PS-*b*-P4VP film also form ordered nanostructures on substrates (Fig. 1b), thus serving as a template for the nanoparticles. This creates a higher degree of control for the nanoparticle formation and arrangement. The diameter of the P4VP cores and the spacing between the adjacent P4VP cores are approximately 29 nm and 33 nm, respectively (Fig. 1c). Ionic impurities such as LiOCH₃ may be present in the copolymer owing to the synthesis process^[30] and interfere with the memory's electrical properties. Hence, the block copolymer of PS-*b*-P4VP (Polymer Source, Inc) first underwent a solvent extraction process (see Experimental) to remove any residual ionic impurities. The "cleaned" PS-*b*-P4VP micelles were then loaded with tetrachloroauric acid (HAuCl₄·3H₂O). AuCl₄⁻ ions were bound as counterions in the polar core of the micelles by protonating the pyridine units. The solution was then treated with hydrazine monohydrate, which resulted in the reduction of Au³⁺ ions and their nucleation to form elemental Au particles in micelle cores (Fig. 1a). The oxidation state of the Au nanoparticles was further confirmed through X-ray photoelectron spectroscopy (see Fig. S1 of the Supporting Information). The binding energies of the doublet for Au 4f_{7/2} (83.7 eV) and 4f_{5/2} (87.4 eV) are characteristic of Au⁰, indicating the presence of elemental Au only. The Au nanoparticles that are generated in the P4VP core are (13 ± 2) nm in diameter (Fig. 1d; molar ratio of HAuCl₄/pyridine units is 0.1). Considering the size of the

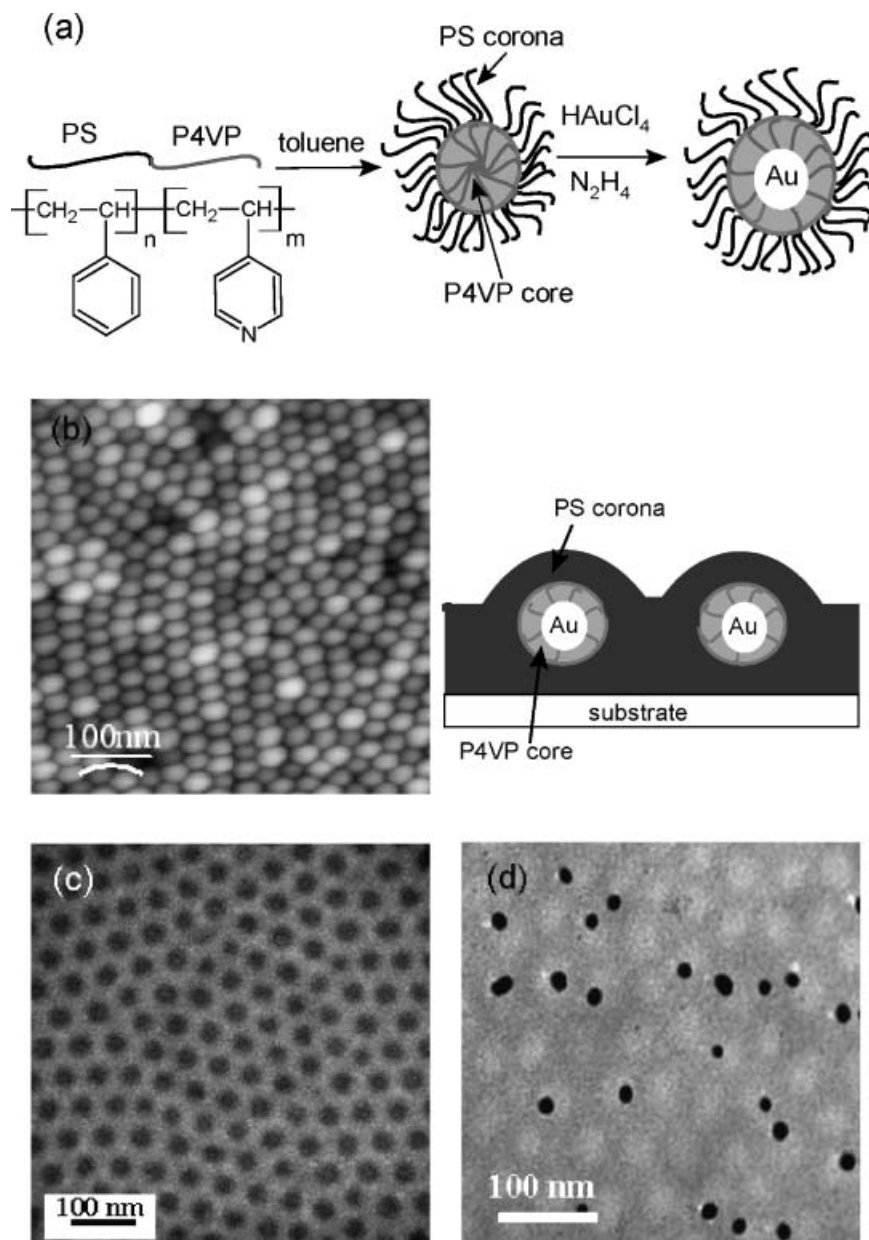


Figure 1. a) Molecular structure of the PS-*b*-P4VP copolymer and a schematic illustration of the micellation process with in situ synthesis of Au nanoparticles in PS-*b*-P4VP. b) Topography image of the surface (from atomic force microscopy) of a spin-coated PS-*b*-P4VP film along with a schematic illustration of a self-assembled PS-*b*-P4VP (with Au nanoparticles) micellar film on a substrate. c) Transmission electron microscopy (TEM) image of PS-*b*-P4VP. The copolymer film is made up of a continuous bright PS matrix and dark spherical P4VP cores. d) TEM image of PS-*b*-P4VP with Au nanoparticles; PS-*b*-(P4VP/Au). The molar ratio of HAuCl₄:P4VP is 0.1.

Au nanoparticles, loading of the Au precursors, and the total number of micelles in the system, the density of the Au nanoparticles is calculated to be around $2.6\text{--}6.7 \times 10^{10} \text{ cm}^{-2}$.

The electrical properties of the copolymer films were studied using a metal–insulator–silicon (MIS) structure (inset of Fig. 2a). The MIS control sample comprising "cleaned" PS-*b*-P4VP

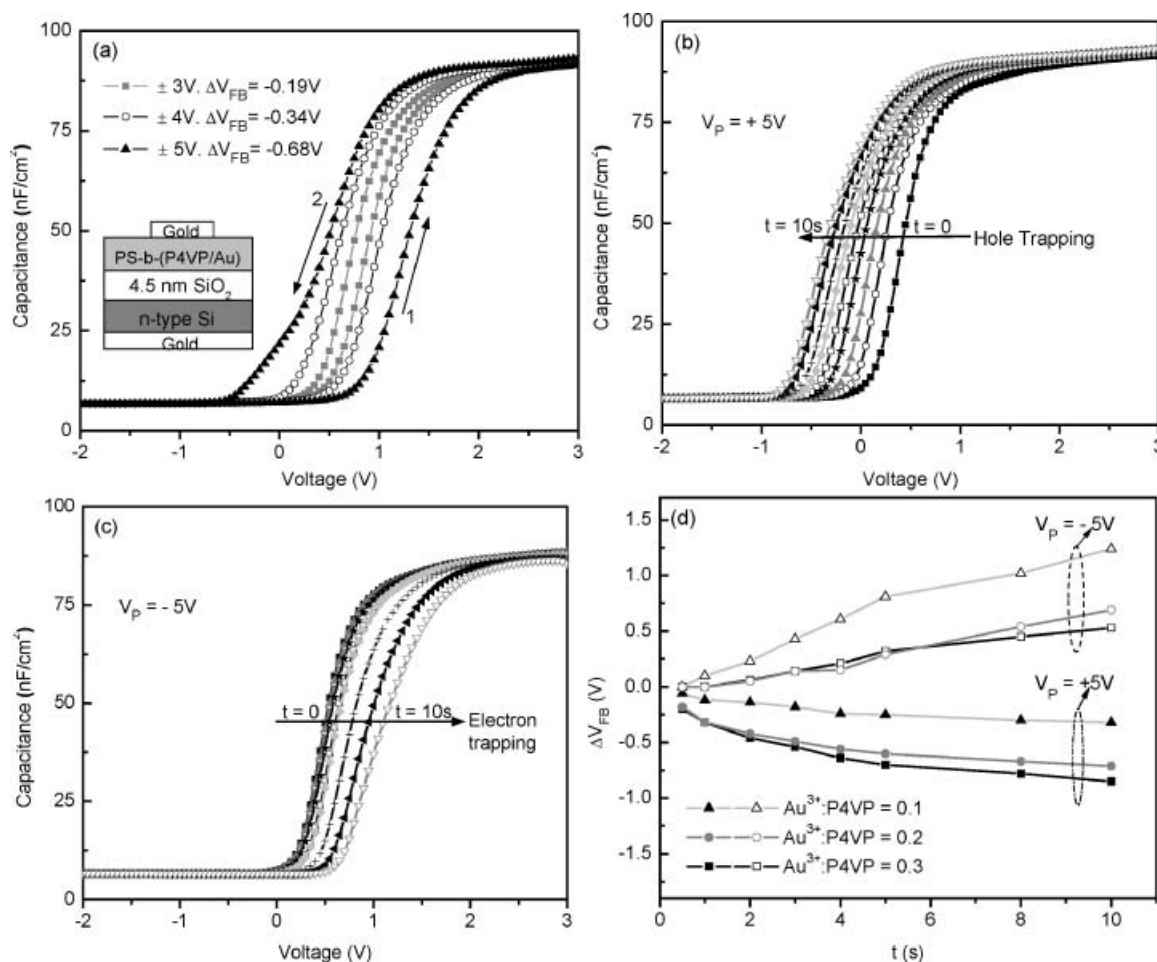


Figure 2. Capacitance–voltage (C–V) measurements at 100 kHz on a MIS structure with a PS-*b*-(P4VP/Au) film. a) Double-sweep C–V characteristics. The C–V hysteresis window increases from -0.19 V to -0.34 V and to -0.68 V upon increasing the operation bias from ± 3 V to ± 4 V and to ± 5 V, respectively. The molar ratio of HAuCl₄:P4VP is 0.1. The inset shows a schematic illustration of the MIS (metal/PS-*b*-(P4VP/Au)/4.5 nm SiO₂/n-type silicon substrate) structure. The voltage bias is applied from the top Au electrode. b,c) Dependence of C–V curves on the accumulated charging time (t) under a pulse voltage (V_p) of $+5$ V and -5 V, respectively. t ranges from 0, 1, 2, 3, 4, 5, 8, and 10 s. For (b), the C–V curve shifts from right to left when t increases while for (c), the C–V curve shifts from left to right when t increases. The voltage sweeping range is ± 3 V. The molar ratio of HAuCl₄:P4VP is 0.2. d) Flat band voltage shift as a function of different charging times (t) for different loadings of the Au nanoparticles (molar ratio of HAuCl₄:P4VP = 0.1, 0.2, and 0.3) at V_p of $+5$ V and -5 V, respectively.

film displayed hysteresis-free C–V characteristics (Fig. S2, Supporting Information), where the hysteresis is defined to be the shift in the flat band voltage (ΔV_{FB}), indicating the absence of any charge trapping events inside PS-*b*-P4VP and its interface. The hysteresis-free C–V curve is also independent of the scan direction and speed (10 – 100 mV s^{−1}). In contrast, the MIS structure with PS-*b*-(P4VP/Au) film yields a ΔV_{FB} of -0.19 V (Fig. 2a, for a 0.1 molar ratio of HAuCl₄ per P4VP unit). This hysteresis window indicates a charge-trapping effect, while the negative shift in V_{FB} implies that holes are predominantly trapped while double-sweeping the device within the ± 3 V range. The magnitude of ΔV_{FB} was dependent on the voltage sweeping range, with the memory window increasing from -0.19 to -0.68 V when the sweeping range amplitude was increased from ± 3 to ± 5 V, indicating an

increased charge injection. Because a charge trapping effect was absent in the MIS control sample, the origin of charge trapping in the PS-*b*-(P4VP/Au) MIS structures is attributed to the Au nanoparticles and/or interface states between the Au nanoparticles and P4VP units. The charge transport between the gold nanoparticles via the block copolymer nanodomains has been found to be a tunneling process.^[31] Tunneling phenomena between nanoparticles and polymer have also been observed by many others.^[32–34] These experimental results suggest that, under the influence of a positive voltage applied to the top gold electrode, holes can be injected and stored in the Au nanoparticles and/or their interface states by a tunneling process through the PS and P4VP layer. When the voltage is swept to a negative value, from $+3$ to -3 V, electron trapping will occur in the Au nanoparticles, resulting in a shift

in capacitance characteristics. The charge density Q accumulated in the Au nanoparticles can be estimated^[35] from $Q \approx C_i \Delta V_{FB}$, where C_i is the capacitance value of the dielectric stack layer. For instance, the voltage shift of -0.19 V at a ± 3 V sweep corresponds to a hole charge density of $9.07 \times 10^{10} \text{ cm}^{-2}$. Using $2.61 \times 10^{10} \text{ cm}^{-2}$ as the density of the gold nanoparticles, one can estimate the average charge per Au nanoparticle for the given system to be around 3 holes per Au nanoparticle. This is comparable to existing few-electron memory devices that use Au nanocrystals embedded in a silicon dioxide matrix.^[36,37]

The effect of the Au nanoparticle loading on the memory effect has also been studied. For an operating voltage of ± 5 V, it was observed that the C - V hysteresis window widens from -0.68 V to -1.47 V to -1.58 V with an increase in the Au nanoparticle concentration (corresponding to 0.1, 0.2, and 0.3 molar ratios of HAuCl₄ per P4VP unit), thus indicating the occurrence of strong carrier trapping with increasing Au concentration. A pulsing experiment was employed for these three different Au nanoparticles concentrations in the MIS configuration. For example, Figure 2 presents the ΔV_{FB} after application of a positive (Fig. 2b) and negative (Fig. 2c) pulse voltage of 5 V to the top gold electrode (for a 0.2 molar ratio of HAuCl₄ per P4VP unit). Generally, upon application of a $+5$ V pulse voltage, the observed negative shift in V_{FB} reflects a net positive charging in the system, which is attributed to hole injection into the confined states of the Au nanoparticles and/or interface states between Au nanoparticle and P4VP units. A charging time of 500 ms leads to a ΔV_{FB} of -0.18 V, and a subsequent charging process leads to continuous negative shift in ΔV_{FB} implying increasing hole trapping events. On the other hand, application of the pulse voltage of -5 V leads to an injection of electrons from the top gold electrode, thus resulting in a positive V_{FB} . The ΔV_{FB} resulting from electron injection is lesser as compared to the ΔV_{FB} resulting from hole injection. This might be due to a higher electron injection barrier (the LUMO level of P4VP lies around 3.5 eV,^[38,39] while the work function of top gold electrode is around 5.1 eV), which in turn leads to a reduced electron tunneling probability.^[40] The effect of the higher electron tunneling barrier was also observed in retention studies (not shown) where the loss rate of electrons was lower than that of holes (HOMO level of P4VP is reported to be around 5.8–6.3 eV^[39,41]). This is because a higher electron tunneling barrier will also mean that the energy barrier height seen by the trapped electrons inside the Au nanoparticle will be higher. Another possibility for the smaller electron-injection effect into the Au nanoparticles might be due to the electron-accepting nature of P4VP,^[42] which may allow easier electron conduction through the micelle cores. As noted in Figure 2d, which summarizes the ΔV_{FB} after the pulsing experiment for various Au nanoparticles loading in the system, electron trapping is more significant for the device using a lower concentration of Au nanoparticles. This might be due to the fact that for lower Au nanoparticle concentrations there is a lesser chance of electron conduction between neighboring Au

particles. This was also observed in current–voltage measurements, where enhanced conductivity occurred for higher concentrations of Au nanoparticles (data available as Supporting Information; Fig. S3). Li et al.^[31] have also recently reported an increase in electron tunneling constant and conductivity with increasing Au nanoparticle concentrations in PS-*b*-P4VP, which was due to a decrease in interparticle distances.

To explore the capability of this active memory layer, an organic memory device comprising a MPIS structure, with pentacene as the active semiconductor layer, was fabricated. Such architecture is an integral part of a typical organic field-effect transistor structure, which can therefore be extended to a floating-gate organic memory transistor. A schematic illustration of the MPIS device is shown in the inset of Figure 3a. In this MPIS device, the gate electrode refers to the heavily doped silicon substrate at the bottom. It can be clearly seen in the C - V curve that the high capacitance of the accumulation region of p-type pentacene occurs when negative gate bias is applied and the low capacitance of the depletion regime occurs at positive gate biasing. It is evident that a significant clockwise C - V hysteresis (i.e., net hole trapping) occurs for all operating bias ranges, indicative of clear memory effects (Fig. 3a). Figure 3b shows the C - V characteristics at various measuring frequencies (50 kHz–1 MHz) and it is observed that the C - V hysteresis window is independent of the applied frequency. The frequency dependence of interface traps is due to their inability to respond completely at higher frequencies, and the frequency-independent behavior observed here indicates that the interface traps that may exist at the interfaces between the pentacene layer, PS-*b*-P4VP, and the thermal oxide, do not make any contribution to the charging process.^[35] Conductance–voltage (G - V) characteristics are presented in the inset of Figure 3b, where a single conductance peak is observed in two directions and at all the measured frequency ranges, indicating trapping and detrapping events of the charge carriers.^[43] In accumulation (negative voltage applied to the bottom silicon substrate), holes may be injected from the pentacene to the Au nanoparticles and/or interface states around the Au nanoparticles via tunneling through the PS block layer. Control samples of pentacene with PS-*b*-P4VP (without Au nanoparticles), did not display any charge-trapping behavior, as shown in the Supporting Information (Fig. S4), further confirming that the Au nanoparticles play the major role for charge storage of the holes from pentacene, acting as deep trapping sites. Upon applying a positive bottom gate voltage, the stored charges in the Au nanoparticles are flushed out, resulting in a flat band voltage shift. The proposed potential charge transfer mechanism is schematically shown in Figure 4a.

The inset of Figure 4b demonstrates the typical high frequency C - V curves of the MPIS memory device under programming and erasing modes. The initial memory device displayed a V_{FB} of -0.5 V. When the memory device is pulsed at negative gate voltage ($V_G = -15$ V) for 500 ms, defined as a program operation, holes from the pentacene layer tunnel

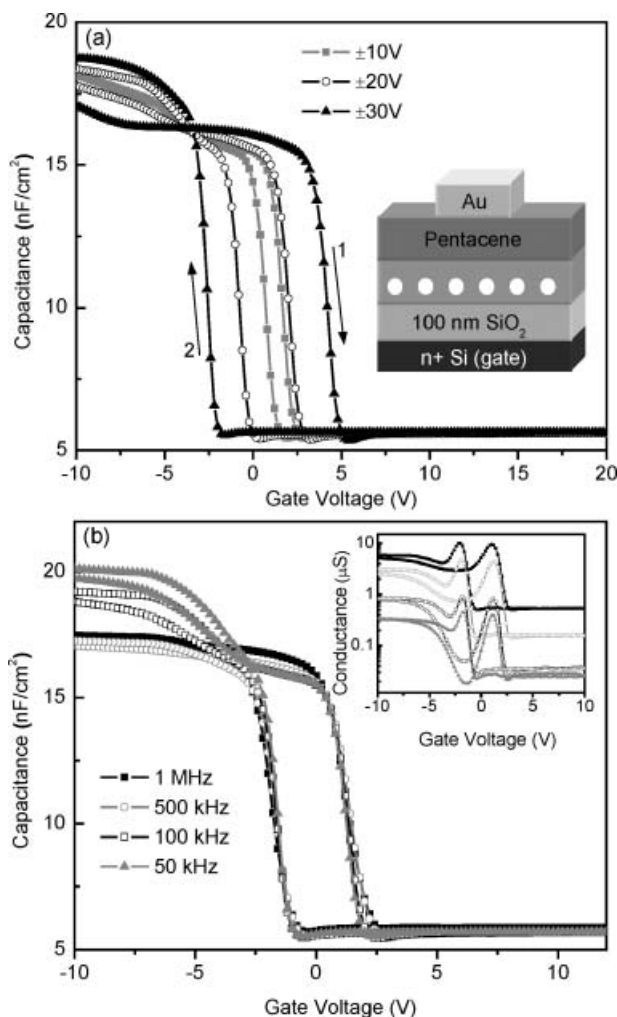


Figure 3. a) Double-sweep C - V characteristics at 100 kHz on an organic memory MPIS device. The hysteresis window increases from 1.0 V to 2.6 V and to 6.8 V upon sweeping the gate voltage from ± 10 V, ± 20 V, and ± 30 V, respectively. The inset shows a schematic structure of a MPIS using PS-*b*-P4VP with Au nanoparticles as floating gate memory elements. The gate voltage is applied to the heavily doped bottom silicon substrate. b) Frequency-dependent C - V characteristics of the organic memory device. The inset shows the corresponding conductance-voltage (G - V) characteristics from 50 kHz to 1 MHz. Molar ratio of HAuCl_4 :P4VP is 0.2.

through the PS layer and are trapped in the Au nanoparticles. The resulting C - V curve demonstrates a negative V_{FB} of 2 V. Subsequently, the programmed C - V curve is pulsed at $V_G = +30$ V for 500 ms, illustrating an erase operation. The C - V curve revealed a ΔV_{FB} of +0.1 V away from the initial one. It is worth nothing that there is no shift in the C - V curve when a pulse of positive gate voltage (when depletion of holes in pentacene layer occurs) is first applied on the initial memory device. This indicates that the source of holes is the pentacene accumulation layer and that there is little influence from interface states and/or mobile ions (if any). The change in flat band voltages under various programming and erasing

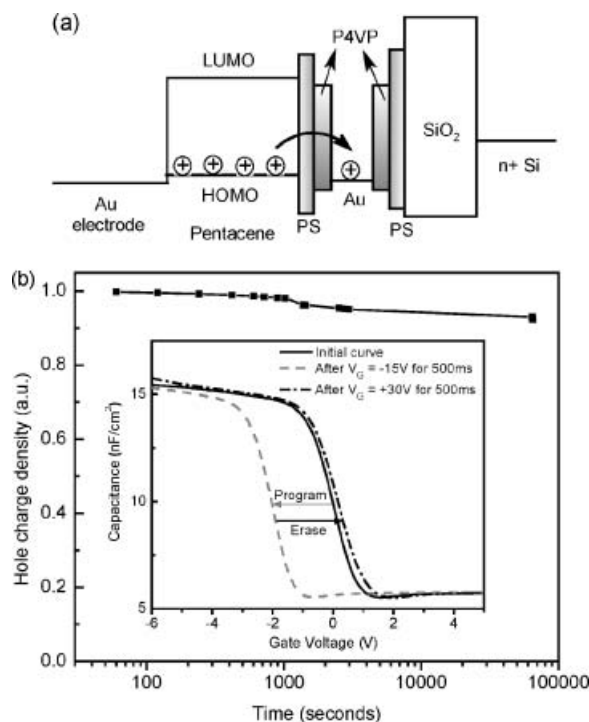


Figure 4. a) Energy level representation for charge transfer and trapping between pentacene and Au nanoparticle in PS-*b*-P4VP. b) Charge retention characteristics (normalized charge density) after the memory device is programmed at -30 V for 500 ms. The inset show the C - V curves of the MPIS memory device at 100 kHz after programming ($V_G = -15$ V for 500 ms) and erasing ($V_G = +30$ V for 500 ms) mode. The gate voltage sweeping range is ± 10 V.

operations can be defined as logic operation of “1” or “0” for a memory device. For the aforementioned program and erase operations, the memory window attains 2.1 V, which is suitable for practical memory applications.

In addition to the ability of Au nanoparticles to store charges from the pentacene layer, data retention is of utmost importance for non-volatile memory applications. Possible charge loss mechanisms during retention include vertical charge loss through the dielectric stack or lateral charge diffusion among the Au nanoparticles. The memory data retention characteristics at room temperature for this nanoparticle floating gate organic memory capacitor are displayed in Figure 4b. The memory capacitor was first charged for 500 ms at a “write” voltage of -30 V and the time dependence of the ΔV_{FB} is evaluated by sweeping the gate voltage from $+10$ V to -10 V. The measured ΔV_{FB} was then expressed in terms of hole charge density correspondingly. A retention ability of ca. 92% was observed after 60000 seconds, confirming that this device has the potential to be considered for non-volatile memory applications. It is believed that the retention ability can be further enhanced by increasing the volume fraction of PS and/or P4VP block to increase the potential energy barrier seen by the trapped charges.

In summary, this work highlighted the versatility of using self-assembled block copolymer with in situ room-temperature synthesis of Au nanoparticles, in the copolymer matrix, which represents an effective approach for polymer memory fabrication. We believe that our work acts as a proof-of-concept, demonstrating the vast potential of these fascinating nanoscaled arrays of nanoparticles. Moreover, we demonstrate the ability to tune the memory behavior by controlling the loading of Au nanoparticles. A memory structure with pentacene as the organic semiconductor exhibited a clockwise $C-V$ hysteresis, indicating a net hole trapping effect. This novel structure displays a large memory window of 2.1 V after writing and erasing modes and a long charge retention ability of ca. 92% over 60000 seconds. This approach, by virtue of its simplicity in design and processing, can realize integrated memory devices and circuits in low-cost plastic electronics applications.

Experimental

Materials: PS-*b*-P4VP diblock copolymers ($M_n^{PS} = 11\,800\text{ kg mol}^{-1}$, $M_n^{P4VP} = 15\,000\text{ kg mol}^{-1}$, $M_w/M_n = 1.04$) were obtained from Polymer Source, Inc.. Pentacene (sublimed) and tetrachloroauric acid ($\text{HAuCl}_4 \cdot 3\text{H}_2\text{O}$) were purchased from Sigma-Aldrich Company.

Solvent Extraction Process of PS-*b*-P4VP: The purification process of the copolymer was done by dissolving the “as-purchased” PS-*b*-P4VP in toluene and washing the copolymer solution with de-ionized water. The water phase was then removed and the toluene phase containing the PS-P4VP was precipitated from hexane. The final precipitate was dried at 50 °C under vacuum for 48 h.

Synthesis of Gold Nanoparticles: The “cleaned” PS-*b*-P4VP precipitate was re-dissolved in toluene (5 mg mL⁻¹). Tetrachloroauric acid ($\text{HAuCl}_4 \cdot 3\text{H}_2\text{O}$) was added to the block copolymer solution in the required amounts given in molar relation to the P4VP units. The molar ratios of HAuCl_4 /pyridine units in the final solutions are 0.1, 0.2, and 0.3, respectively. The solutions were subsequently stirred for 24 h and then treated with hydrazine monohydrate (ratio of $\text{N}_2\text{H}_4 \cdot \text{H}_2\text{O}:\text{Au}^{3+} = 1:1$). The Au^{3+} ions were reduced and nucleated to form elemental gold particles in micelle cores. The oxidation state of the Au nanoparticles was also confirmed through X-ray photoelectron spectroscopy with monochromatic Al K α radiation source (1486.6 eV photons, 150 W).

Device Fabrication: The MIS or MPIS structures were fabricated on n-type silicon wafer with 4.5 nm or 100 nm thermally grown silicon dioxide (SiO_2) on top, respectively. A 30 nm thick micellar film of self-assembled PS-*b*-P4VP or 50 nm thick micellar film of self-assembled PS-*b*-P4VP with Au nanoparticles was spun coat on top of the SiO_2 -silicon substrate. The thickness of the copolymer films and diameter of the micelles were measured by utilizing Atomic Force Microscopy (Digital Instruments Dimension 3000). After spin-coating, the copolymer film was annealed at 110 °C in vacuum for 72 hours. The pentacene was thermally evaporated, at a deposition rate of 0.1 nm s⁻¹ and a pressure of 10⁻⁷ Torr (1 Torr = 1.333 × 10² Pa), to form a 45 nm thick film. A top metal electrode of gold was subsequently deposited by thermal evaporation through a shadow mask of 0.3 mm diameter size. The substrate backside was coated with a layer of gold after removing the backside oxide to form an ohmic contact.

Electrical Characterization: All electrical measurements were done in vacuum environment (10⁻⁴ Torr). Capacitance–voltage ($C-V$) and conductance–voltage ($G-V$) measurements were done with a HP 4284A Precision LCR Meter at the frequency of 100 kHz and an ac amplitude of 15 mV was superimposed on the dc bias. Current–voltage

characteristics were measured with a Keithley 4200 semiconductor characterization system.

Received: October 12, 2007

Revised: December 26, 2007

Published online: May 15, 2008

- [1] M. Böltau, S. Walheim, J. Mlynek, G. Krausch, U. Steiner, *Nature* **1998**, 391, 877.
- [2] M. J. Fasolka, D. J. Harris, A. M. Mayes, M. Yoon, S. G. J. Mochrie, *Phys. Rev. Lett.* **1997**, 79, 3018.
- [3] I. W. Hamley, in *Block Copolymers in Solution: Fundamentals and Applications*, Wiley, Hoboken, NJ **2005**, Ch. 6.
- [4] H. Otsuka, Y. Nagasaki, K. Kataoka, *Curr. Opin. Colloid Interface Sci.* **2001**, 6, 3.
- [5] T. W. Chung, K. Y. Cho, H.-C. Lee, J. W. Nah, J. H. Yeo, T. Akaike, C. S. Cho, *Polymer* **2004**, 45, 1591.
- [6] J. Spatz, S. Mößmer, M. Möller, M. Kocher, D. Neher, G. Wegner, *Adv. Mater.* **1998**, 10, 473.
- [7] M. Antonietti, E. Wenz, L. Bronstein, M. Seregina, *Adv. Mater.* **1995**, 7, 1000.
- [8] G. Kästle, H.-G. Boyen, F. Weigl, G. Lengel, T. Herzog, P. Ziemann, S. Riethmüller, O. Mayer, C. Hartmann, J. P. Spatz, M. Möller, M. Ozawa, F. Banhart, M. G. Garnier, P. Oelhafen, *Adv. Funct. Mater.* **2003**, 13, 853.
- [9] B.-H. Sohn, S.-I. Yoo, B.-W. Seo, S.-H. Yun, S.-M. Park, *J. Am. Chem. Soc.* **2001**, 123, 12734.
- [10] A. Haryono, W. H. Binder, *Small* **2006**, 2, 600.
- [11] S. Förster, M. Antonietti, *Adv. Mater.* **1998**, 10, 195.
- [12] L. Qi, H. Cölfen, M. Antonietti, *Nano Lett.* **2001**, 1, 61.
- [13] J. Turkevitch, P. C. Stevenson, J. Hillier, *Discuss. Faraday Soc.* **1951**, 11, 55.
- [14] M.-C. Daniel, D. Astruc, *Chem. Rev.* **2004**, 104, 293.
- [15] Y.-W. Jun, S.-M. Lee, N.-J. Kang, J. Cheon, *J. Am. Chem. Soc.* **2001**, 123, 5150.
- [16] F. Wang, G. Xu, Z. Zhang, X. Xin, *Eur. J. Inorg. Chem.* **2006**, 109.
- [17] M. Brust, M. Walker, D. Bethell, D. J. Schiffrin, R. Whyman, *J. Chem. Soc. Chem. Commun.* **1994**, 801.
- [18] R. J. Tseng, J. Huang, J. Ouyang, R. B. Kaner, Y. Yang, *Nano Lett.* **2005**, 5, 1077.
- [19] J. Ouyang, C.-W. Chu, C. R. Szmanda, L. Ma, Y. Yang, *Nat. Mater.* **2004**, 3, 918.
- [20] L. D. Bozano, B. W. Kean, M. Beinhoff, K. R. Carter, P. M. Rice, J. C. Scott, *Adv. Funct. Mater.* **2005**, 15, 1933.
- [21] D. Tondelier, K. Lmimouni, D. Vuillaume, *Appl. Phys. Lett.* **2004**, 85, 5763.
- [22] Y. Yang, J. Ouyang, L. Ma, R. J.-H. Tseng, C.-W. Chu, *Adv. Funct. Mater.* **2006**, 16, 1001.
- [23] M. Cölle, M. Büchel, D. M. de Leeuw, *Org. Electron.* **2006**, 7, 305.
- [24] W. Tang, H. Shi, G. Xu, B. S. Ong, Z. D. Popovic, J. Deng, J. Zhao, G. Rao, *Adv. Mater.* **2005**, 17, 2307.
- [25] S. Paul, C. Pearson, A. Molloy, M. A. Cousins, M. Green, S. Kollipoulou, P. Dimitrakakis, P. Normand, D. Tsoukalas, M. C. Petty, *Nano Lett.* **2003**, 3, 533.
- [26] W. L. Leong, P. S. Lee, S. G. Mhaisalkar, T. P. Chen, A. Dodabalapur, *Appl. Phys. Lett.* **2007**, 90, 042906.
- [27] J. G. Simmons, R. R. Verderber, *Proc. R. Soc. London Ser. A* **1967**, 301, 77.
- [28] J. C. Scott, L. D. Bozano, *Adv. Mater.* **2007**, 19, 1452.
- [29] G. Gelinck, *Nature* **2007**, 445, 268.
- [30] S. K. Varshney, X. F. Zhong, A. Eisenberg, *Macromolecules* **1993**, 26, 701.
- [31] C.-P. Li, C.-H. Wu, K.-H. Wei, J.-T. Sheu, J. Y. Huang, U.-S. Jeng, K. S. Liang, *Adv. Funct. Mater.* **2007**, 17, 2283.

- [32] C. Laurent, E. Kay, N. Souag, *J. Appl. Phys.* **1998**, *64*, 336.
- [33] V. Torma, O. Vidoni, U. Simon, G. Schmid, *Eur. J. Inorg. Chem.* **2003**, 1121.
- [34] U. Simon, *Adv. Mater.* **1998**, *10*, 1487.
- [35] E. H. Nicollian, J. R. Brews, in *MOS (Metal Oxide Semiconductor) Physics and Technology*, Wiley, New York **1982**, Ch. 7–10.
- [36] C. Lee, U. Ganguly, V. Narayanan, T.-H. Hou, J. Kim, E. C. Kan, *IEEE Electron Devices Lett.* **2005**, *26*, 879.
- [37] W. Guan, S. Long, M. Liu, Z. Li, Y. Hu, Q. Liu, *J. Phys. D* **2007**, *40*, 2754.
- [38] C.-P. Li, K.-H. Wei, J. Y. Huang, *Angew. Chem. Int. Ed.* **2006**, *45*, 1449.
- [39] S. Dailey, M. Halim, E. Rebourt, L. E. Horsburgh, I. D. W. Samuel, A. P. Monlman, *J. Phys. Condens. Matter* **1998**, *10*, 5171.
- [40] Q.-A. Huang, *Appl. Surf. Sci.* **1996**, *93*, 77.
- [41] M. K. Awad, K. S. Khairou, M. A. Diab, *Polym. Degrad. Stab.* **1994**, *46*, 165.
- [42] G. R. Newkome, W. W. Paudler, in: *Contemporary Heterocyclic Chemistry: Syntheses, Reactions and Applications*, Wiley, New York **1982**.
- [43] S. M. Sze, *Physics of Semiconductor Devices*, 2nd ed, Wiley, New York **1981**, Ch. 7.